

# Elucidating Toxicodynamic Differences at the Molecular Scale between ZnO Nanoparticles and ZnCl<sub>2</sub> in *Enchytraeus crypticus* via Nontargeted Metabolomics

Erkai He, Rongliang Qiu, Xinde Cao, Lan Song, Willie J.G.M. Peijnenburg, and Hao Qiu\*



Cite This: *Environ. Sci. Technol.* 2020, 54, 3487–3498



Read Online

ACCESS |



Metrics & More

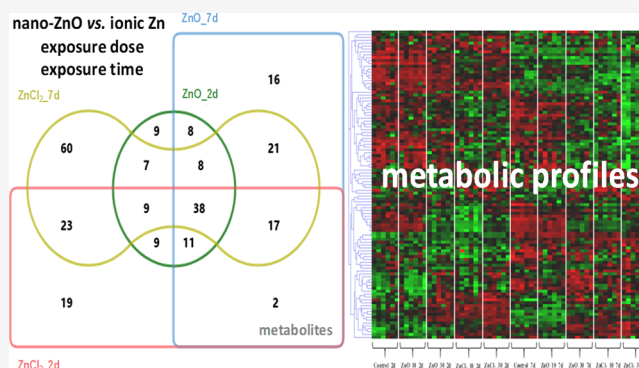


Article Recommendations



Supporting Information

**ABSTRACT:** Much effort has been devoted to clarifying the comparative toxicity of ZnO nanoparticles (NPs) and Zn ions; however, little is known about their toxicodynamic processes at the metabolic level. Here, we investigated the acute (2d) and chronic (7d) effects to a soil species, *Enchytraeus crypticus*, of two sublethal doses of ZnO-NPs and ZnCl<sub>2</sub> (10 and 30 mg/L Zn) using ultrahigh performance liquid chromatography-quadrupole-time-of-flight/mass spectrometry-based metabolomics. The metabolomics analysis identified 99, 128, 121, and 183 significantly changed metabolites (SCMs) in *E. crypticus* exposed to ZnO-NPs for 2d, ZnCl<sub>2</sub> for 2d, ZnO-NPs for 7d, and ZnCl<sub>2</sub> for 7d, respectively, suggesting that ZnCl<sub>2</sub> induced stronger metabolic reprogramming than ZnO-NPs, and a longer exposure time caused greater metabolite changes. Among the SCMs, 67 were shared by ZnO-NPs and ZnCl<sub>2</sub> after 2d and 84 after 7d. These metabolites were mainly related to oxidative stress and antioxidant defense, membrane disturbance, and energy expenditure. The targeted analysis on physiological and biochemical responses further proved the metabolic observations. Nevertheless, 32 (33%) and 37 (31%) SCMs were found only in ZnO-NP treatments after 2 and 7d, respectively, suggesting that the toxicity of ZnO-NPs cannot be solely attributed to the released Zn ions. Metabolic pathway analysis revealed significant perturbations of galactose metabolism, amino sugar and nucleotide sugar metabolism, and glycerophospholipid metabolism in all test groups. Based on involvement frequency, glucose-1-phosphate, glycerol 3-phosphate, and phosphorylcholine could serve as universal biomarkers for exposure to different Zn forms. Four pathways perturbed by ZnO-NPs were nanospecific upon acute exposure and three upon chronic exposure. Our findings demonstrated that metabolomics is an effective tool for understanding the molecular toxicity mechanism and highlighted that time-series measurements are essential for discovering and comparing modes of action of metal ions and NPs.



survival as the toxicological endpoints.<sup>13–15</sup> According to the adverse outcome pathways (AOPs) concept, these organismal effects normally occur at a later stage of toxicity (thus less sensitive) than effects at lower levels of biological organization.<sup>16</sup> Accordingly, the endpoints at the organismal level may not show significant responses at environmentally relevant exposure concentrations.<sup>17</sup> In comparison, the effects at the molecular level are more sensitive and can provide a deeper insight into the subtle responses of complex biological systems under NP stress.<sup>18</sup> Omics-based approaches such as genomics, transcriptomics, proteomics, and metabolomics have been successfully applied in identifying certain molecular responses, which point to the underlying toxic mechanisms and pathways.<sup>12,18–20</sup> Compared to other omics technologies, metabolomics is gaining more attention now than ever before.<sup>21</sup> This is because metabolites are the terminal downstream products of gene expression and represent functional entities, whereas genes and proteins may be affected by epigenetic regulation and posttranslational modifications.<sup>22</sup> In other words, metabolomics represents the final “omic” level in a biological system, which can provide a snapshot of what has certainly happened and is happening in the organism.<sup>19</sup> At present, metabolomic studies regarding nanotoxicity mostly focus on aquatic species<sup>17,23,24</sup> and plants,<sup>19,25,26</sup> and much lesser work has been conducted on soil animals. Moreover, there is often a lack of targeted analysis on the mechanistic effects indicated by metabolic observations.

To obtain a better understanding of the mode of action of NPs, it is equally important to select the appropriate dose and duration of exposure.<sup>27</sup> The majority of previous toxicological studies have been performed by means of short-term exposure to a high dose.<sup>12,28</sup> However, in the natural environment, organisms are more often subject to long-term low-level exposure.<sup>23</sup> The acute exposure of NPs at trace levels may show negligible or limited effect, whereas longer exposure time is valuable for revealing the cumulative effect.<sup>28</sup> Our recent study has demonstrated that exposure of *Enchytraeus crypticus* to low concentrations of ZnO NPs caused no mortality from day 1 to day 4, but an apparent decline in survival rates was observed from day 7 to day 14.<sup>7</sup> Hydrogen-1 NMR-based metabolomic analyses have also revealed heightened *Eisenia fetida* response with prolonged exposure to phenanthrene.<sup>29</sup> From the perspectives of toxicokinetics and toxicodynamics, it is expected that the organism will take certain time to respond to the exposure and then reprogram the levels of metabolites to resist and/or tolerate the toxic effect.<sup>23,30</sup> Hence, it is important to monitor the fluctuations in the metabolic responses of the organisms with time. To our knowledge, applying a dynamic and metabolomic approach to investigate the comparative toxicity of NPs and their ionic counterparts has rarely been done before. Studies exploring this knowledge gap would be useful for clarifying nanotoxicity and for discovering early biomarkers of phenotypic changes.

Against this background, this work examined the acute and chronic effects to a key soil species, *E. crypticus* of two sublethal doses of ZnO-NPs and ZnCl<sub>2</sub> using mass spectrometry-based nontargeted metabolomics. Special attention was paid to (1) identify the differential metabolites and associated biological pathways for both ZnO-NPs and ionic Zn exposures, (2) see whether ZnO-NPs, despite showing the same “invisible” effects as Zn<sup>2+</sup> ions, are able to cause distinct metabolic responses, and (3) determine how time may affect the nature of the difference in metabolic profiles between the different Zn forms.

Regardless of metal forms, a higher exposure dose and a longer exposure duration were expected to induce more apparent metabolic changes. Assuming that the released Zn ions play a dominant role in the toxicity of ZnO-NPs, the metabolic responses of *E. crypticus* to ZnO-NPs would be less pronounced than that to ZnCl<sub>2</sub> at an equivalent concentration of Zn, and this difference may become smaller with increasing exposure time considering the gradual dissolution of ZnO-NPs. The targeted analyses of physiological and biochemical responses as indicated by the metabolic observations were further performed for validation purpose. In addition, previously we showed the different dynamic accumulation and toxicity patterns of ZnO-NPs and ionic Zn in *E. crypticus* at the organismal level.<sup>7</sup> Here, the metabolic reprogramming by *E. crypticus* was linked to the previously reported toxicokinetic and toxicodynamic processes of ZnO-NPs and ionic Zn at the organismal level, which is expected to provide new insights into the mechanisms employed by soil animals to cope with these two different Zn forms.

## MATERIALS AND METHODS

**Test Chemicals.** ZnO-NPs (nominal size <50 nm) and ZnCl<sub>2</sub> (purity > 99%) were obtained from Sigma-Aldrich. Scanning electron microscopy (SEM) and dynamic light scattering were used for the characterization of ZnO-NPs, and the results were reported in our previous study.<sup>7</sup> In brief, the SEM image demonstrated that ZnO-NPs mainly existed as spherical particles with a particle size of 24–48 nm. The hydrodynamic diameters of the ZnO-NPs increased from 258 ± 12 to 1500 ± 275 with the increasing incubation time (0, 1, 5, 24, 96, and 168 h) (see Table S1 for details).

**Test Organism.** The ecologically relevant soil-living worm, *E. crypticus* (Oligochaeta: Enchytraeidae) was used as the test species. The sensitivity to various stressors, well-characterized genome, ease of maintenance, and short reproduction cycle make it a preferred model species for toxicological studies.<sup>31,32</sup> The worms were maintained on an agar gel medium in a climate chamber (20 °C, 75% relative humidity, and complete darkness). Oatmeal and yolk powder were provided regularly as the food source.<sup>7</sup> Adult worms (body length: 0.8–1.2 cm, wet weight: 1.0–1.5 mg) with clearly visible clitellum were used for the toxicity tests.

**Toxicity Tests.** Toxicities of ZnO-NPs and ZnCl<sub>2</sub> to *E. crypticus* were studied using a simulated soil solution-quartz sand system. The simulated soil solution was mainly composed of 0.2 mM CaCl<sub>2</sub>, 2.0 mM NaCl, 0.05 mM MgSO<sub>4</sub>, and 0.078 mM KCl. The preparation of this exposure medium was described in detail elsewhere.<sup>33</sup> The worms were exposed to different levels of Zn (0, 10, and 30 mg/L) spiked with ZnO-NPs and ZnCl<sub>2</sub> for 2 and 7 days, separately (denoted as: Control\_2d, ZnO\_10\_2d, ZnO\_30\_2d, ZnCl<sub>2</sub>\_10\_2d, ZnCl<sub>2</sub>\_30\_2d, Control\_7d, ZnO\_10\_7d, ZnO\_30\_7d, ZnCl<sub>2</sub>\_10\_7d, and ZnCl<sub>2</sub>\_30\_7d). In our previous study, we have shown that the 7 days LC50 of ZnO-NPs and ZnCl<sub>2</sub> were 72 and 62 mg/L of Zn, respectively, for *E. crypticus* in the same exposure system, and no mortality was observed at concentrations up to approximately 30 mg/L of Zn.<sup>7</sup> In the present study, the toxicity exposure was performed in a glass jar filled with 20.0 g quartz sand and 5.5 mL test solution containing different concentrations of Zn. Twenty worms were introduced into each glass jar and six replicates were used for each treatment. In order to meet the quantity requirement for metabolite analysis, each replicate was composed of four jars,

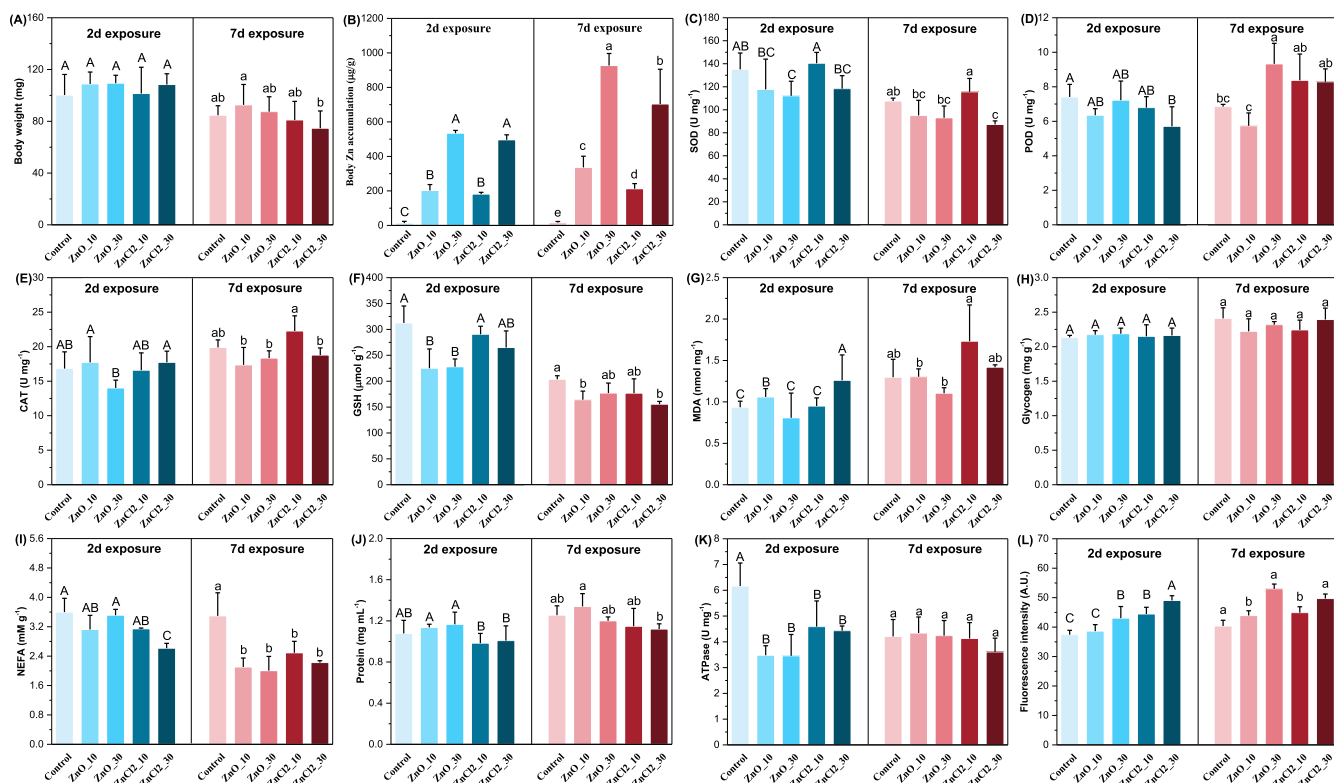


**Figure 1.** Changes in body weights (A), body Zn accumulation (B), SOD (C), POD (D), CAT (E), GSH (F), MDA (G), glycogen (H), NEFA (I), protein (J), ATPase (K), and relative fluorescence intensity (L) of *E. crypticus* exposed to different concentrations of ZnO-NPs and ZnCl<sub>2</sub> (0, 10, and 30 mg Zn/L) for 2 and 7 days, respectively. Body weights were obtained by weighing the pooled samples (80 individuals) in each replicate. The values labeled with the same letter are not significantly different at  $p < 0.05$  level by Tukey's post-hoc test.

that is, in total  $20 \times 4 = 80$  individuals. The tests were run in the climate chamber at 20 °C, 75% relative humidity, and a cycle of 16 h light-8 h dark. During the experiment, the jars were weighed daily and demineralized water was added to replenish water loss. At the end of the test, no mortality of worms was observed. The surviving worms were collected, weighed, frozen with liquid N<sub>2</sub>, and stored at -80 °C for further analysis. Body Zn concentration was analyzed using inductively coupled plasma-mass spectrometry (ICP-MS) after acid digestion of freeze dried worms.

**Metabolite Extraction and Ultrahigh Performance Liquid Chromatography-Quadrupole-Time-of-Flight/Mass Spectrometry Analysis.** For the extraction of metabolites, each pooled sample containing ~80 individuals (80–120 mg) was thawed at 4 °C. Then, 200 µL of ultrapure water and 800 µL of methanol/acetonitrile (1:1, v/v) were added to each sample which was homogenized by an MP homogenizer (6.0 m/s, 60 s, twice). The homogenate was sonicated twice (30 min/once) at low temperature (0–4 °C); the mixture was then centrifuged for 15 min (13,000 rpm, 4 °C). The collected supernatant was dried in a vacuum centrifuge and stored at -80 °C. Before the analysis of metabolites, the samples were redissolved in 100 µL of an acetonitrile/water (1:1, v/v) solvent. Quality control (QC) samples were prepared by mixing equal aliquots of all samples of different treatments.

Metabolite profiling of *E. crypticus* was performed using ultrahigh performance liquid chromatography (UHPLC) (1290 Infinity LC, Agilent Technologies) coupled with quadrupole time-of-flight (Q-TOF) (AB Sciex TripleTOF 6600). All samples used for metabolomics were analyzed as a

single batch in a random order. The QC samples were injected once for every 10 samples to monitor and evaluate the stability of the system and the reliability of the experimental data. Electrospray ionization (ESI) was used for mass detection. Mass spectra were acquired in both ESI cationic and anionic modes. The operational conditions of the equipment and data acquisition are described in Text S1.

**Data Processing and Statistical Analysis.** After data normalization (Pareto scaling) and data transformation (log transformed), principal component analysis (PCA) and partial least-squares-discriminant analysis (PLS-DA) were run using SIMCA-P 14.1 (Umetrics, Umea, Sweden). PCA was used to reduce the complexity of metabolites data matrix and to summarize the similarities and differences between each sample group. PLS-DA is a supervised clustering method, which uses a multiple linear regression technique to maximize the separation between groups and helps to understand which variables carry the class separating information.<sup>34</sup> The variable importance in projection (VIP) value of each variable in the PLS-DA model was calculated to indicate its contribution to the classification. Metabolites with VIP value > 1.0 and  $p$  value < 0.05 (one-way ANOVA) were regarded as the ones that were significantly influenced by Zn exposure.

Multiple Experiment Viewer (MeV 4.9) was used for hierarchical clustering analysis of the relative expression data of the identified metabolites. Heatmap was presented as a visual aid to show the trend of metabolite change. The identified discriminating metabolites were further analyzed to determine the relevant biological pathways using MetaboAnalyst 3.0 (<http://www.metaboanalyst.ca/>), which combines results from powerful pathway enrichment analysis with

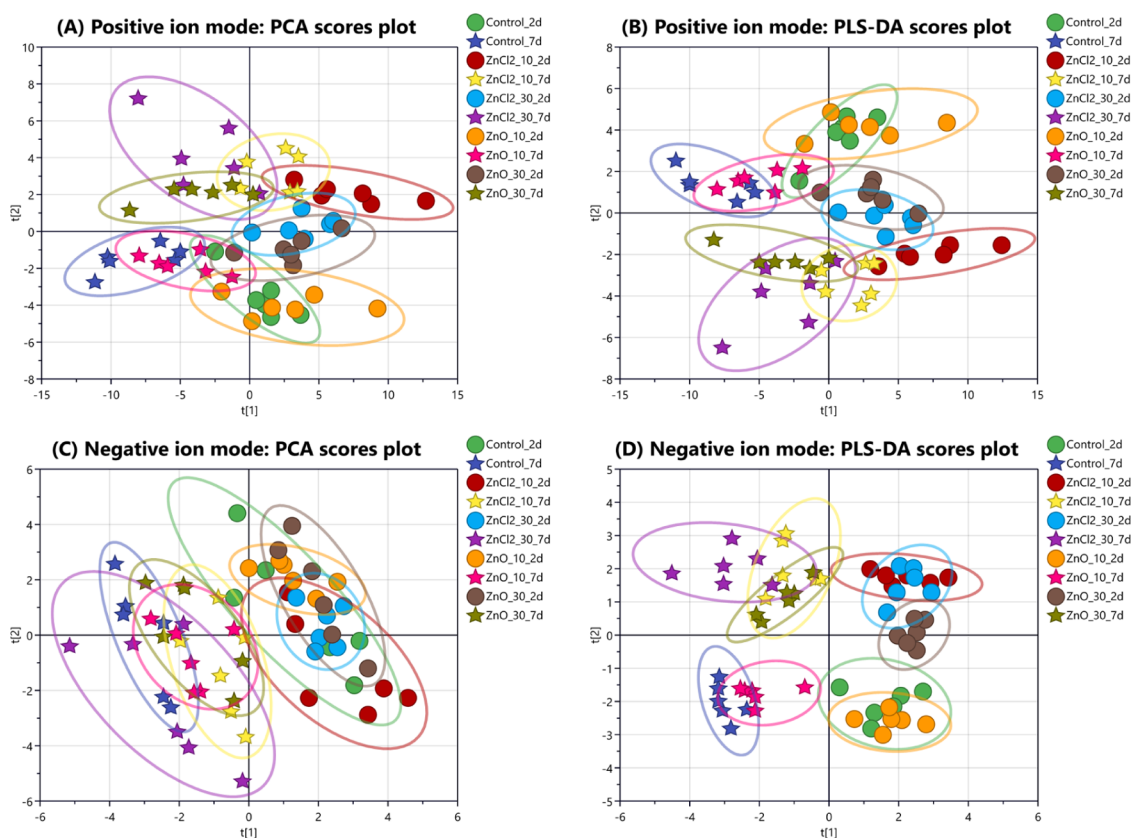


**Figure 2.** PCA and PLS-DA of the metabolic profiles in *E. crypticus* exposed to different concentrations of ZnO-NPs and ZnCl<sub>2</sub> (0, 10, and 30 mg Zn/L) for 2 and 7 days, respectively. Positive ion mode (A,B):  $R^2X_{cum} = 0.648$ ,  $Q_{cum}^2 = 0.552$  for PCA,  $R^2X_{cum} = 0.704$ ,  $R^2Y_{cum} = 0.759$ ,  $Q_{cum}^2 = 0.415$  for PLS-DA. Negative ion mode (C,D):  $R^2X_{cum} = 0.598$ ,  $Q_{cum}^2 = 0.368$  for PCA,  $R^2X_{cum} = 0.279$ ,  $R^2Y_{cum} = 0.208$ ,  $Q_{cum}^2 = 0.182$  for PLS-DA. Ellipse: Hotelling's T<sub>2</sub> (95%).

pathway topology analysis. The pathways with  $p$  value < 0.05 (enrichment analysis) and impact value > 0.1 (pathway topology analysis) were considered as potentially affected.<sup>35</sup>

**Measurements of Dissolution of ZnO-NPs.** A dissolution experiment was performed to determine the dynamic release of Zn<sup>2+</sup> from ZnO-NPs. The ZnO-NPs treatments with initial concentrations of 10 and 30 mg Zn/L were prepared following the same steps for toxicity tests. For each concentration, seven sampling time points (1 h, 1, 2, 4, 7, 10, and 14 d) were selected to gain a full picture of dissolution dynamics of ZnO NPs. The amount of released Zn ions was determined by ultrafiltration of the stimulated soil solution over a 30 kDa ultrafilter (Sartorius) and centrifugation at 4000 rpm for 25 min.<sup>36</sup> In this way, the ZnO particles were retained on the filter, whereas the released Zn<sup>2+</sup> were determined by measuring the Zn concentration in the ultrafiltrate with ICP-MS.

**Measurements of Oxidative Stress, Energy Reserve, and Membrane Integrity.** In a parallel exposure experiment, the oxidative stress-related (superoxide dismutase (SOD), peroxidase (POD), catalase (CAT), glutathione (GSH), and malondialdehyde (MDA)) and energy store-related (glycogen, non-esterified fatty acid (NEFA), and total protein) parameters in the frozen worms were determined by commercial assay kits (Jiancheng Bioengineering Institute, Nanjing, China) according to the manufacturer's instructions ([www.njjc.bio.com](http://www.njjc.bio.com)). Membrane permeability of the surviving *E. crypticus* was examined using confocal laser scanning microscopy (Leica, TCS SP2, Bensheim, Germany) after propidium iodide (PI)

staining.<sup>37</sup> The relative fluorescence intensity was quantified using ImageJ (open source application).

## RESULTS AND DISCUSSION

**Dissolution Dynamics of ZnO-NPs.** The concentrations of dissolved Zn were measured in ZnO-NPs treatments during 14 days of incubation (Table S2). The ZnO-NPs exhibited a gradual dissolution with increasing incubation time, with the percentage of released Zn<sup>2+</sup> in ZnO-NPs treatments of 10 and 30 mg Zn/L increasing from 19 to 31% and from 5 to 11%, respectively. It seemed that a higher concentration of ZnO-NPs resulted in a lower rate of ion release. However, the total quantities of released Zn<sup>2+</sup> at each time point were similar. After 2 days, the concentrations of released Zn<sup>2+</sup> were 2.45 and 2.53 mg/L for the 10 and 30 mg Zn/L ZnO-NPs treatments, respectively. These values were 3.01 and 3.22 after 7 days.

**Body Weight and Body Zn Accumulation.** After exposure for either 2 days or 7 days, there were no significant differences in body weight between the control and Zn-exposed animals (Figure 1A). However, it appeared that increasing the ZnO-NPs or ZnCl<sub>2</sub> concentrations from 10 to 30 mg Zn/L slightly decreased the body weight of the animals at day 7, indicating a possible stress response. Nevertheless, more sensitive endpoints that focus on molecular changes within the organisms are desired and would shed new insights into toxicity mechanisms as compared to the more gross measures such as body weight.<sup>26</sup> The body Zn concentrations of *E. crypticus* increased with increasing exposure duration and exposure concentrations of ZnO-NPs or ZnCl<sub>2</sub> (Figure 1B). At

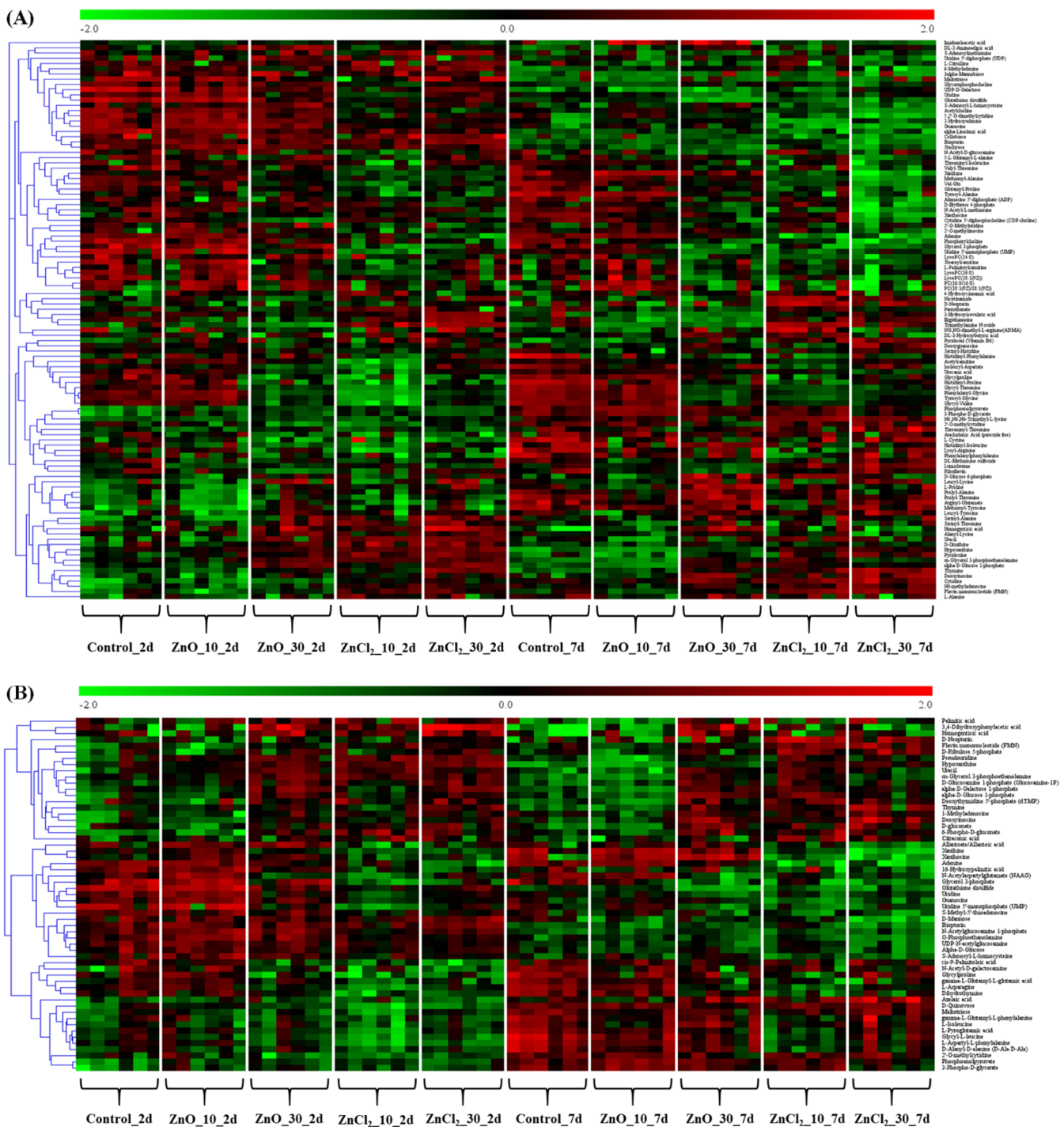


**Figure 3.** Hierarchical clustering of SCMs ( $p < 0.05$  and  $VIP > 1$ ) in *E. crypticus* after exposure to ZnO-NPs and ZnCl<sub>2</sub> at different exposure concentrations and exposure times. Using the normalized relative expression data, 107 metabolites in the positive ion mode (A) and 57 metabolites in the negative ion mode (B) were clustered.

an equivalent Zn exposure, the differences in body Zn concentrations between ZnO-NP- and ZnCl<sub>2</sub>-exposed groups were not statistically significant after short-term exposure ( $p > 0.05$ ), whereas the body Zn concentrations in ZnO-NP-exposed groups were significantly higher than those in the groups exposed to ZnCl<sub>2</sub> after long-term exposure ( $p < 0.05$ ). Dynamic aspects should therefore be considered in understanding the uptake and subsequent toxicity of these two Zn forms.

In a companion study with broader ranges of Zn concentrations and longer exposure time (14 days), the toxicokinetic–toxicodynamic (TK–TD) models have been applied to simulate the processes that lead to ZnO-NPs and ZnCl<sub>2</sub> toxicity at the level of organisms over time.<sup>7</sup> The estimated kinetic parameters of ZnO-NPs and ZnCl<sub>2</sub> in *E. crypticus*, at the exposure concentrations of 10 and 30 mg Zn/L adopted in the present study, were derived (Table S3). For all Zn treatments, the uptake rate constants ( $K_u$ ) were higher than the depuration rate constants ( $K_d$ ). According to the critical

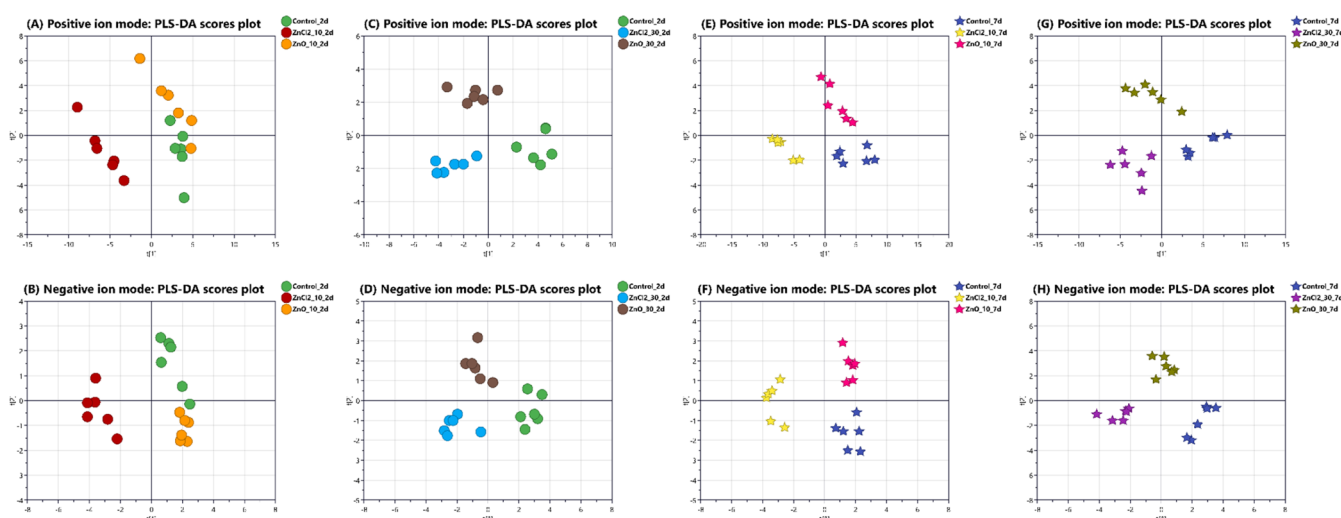


**Figure 4.** PLS-DA of the metabolic profiles in *E. crypticus* exposed to ZnO-NPs and ZnCl<sub>2</sub> at an equivalent concentration of Zn (10 or 30 mg/L) and a single time point (day 2 or 7). Specifically, the grouped comparisons included: Control\_2d vs ZnCl<sub>2</sub>\_10\_2d vs ZnO\_10\_2d (A,B), Control\_2d vs ZnCl<sub>2</sub>\_30\_2d vs ZnO\_30\_2d (C,D), Control\_7d vs ZnCl<sub>2</sub>\_10\_7d vs ZnO\_10\_7d (E,F), and Control\_7d vs ZnCl<sub>2</sub>\_30\_7d vs ZnO\_30\_7d (G,H).

body residue theory, when the rate of metal uptake exceeds the rate of detoxification and depuration, the metal will accumulate in the animals and trigger toxic effects once the critical body metal burden is reached.<sup>38</sup> It has also been recognized that metal detoxification itself is an energy-cost process, which can be witnessed as indirect physiological effects on body weight, reproduction, and survival.<sup>39,40</sup> At the same Zn exposure concentration, the  $K_u$  and  $K_d$  values of ZnO-NPs were smaller than those of ZnCl<sub>2</sub>. The biological half-life was longer for ZnO-NPs than for ZnCl<sub>2</sub>. These results quantitatively reflected the differences in TK–TD processes between nanoparticulate Zn and ionic Zn. The molecular mechanisms for the differences were explored by looking at the metabolic profiles in the animals.

**Metabolic Responses of *E. crypticus* Exposed to ZnO-NPs and ZnCl<sub>2</sub>.** Initially, unsupervised PCA was performed on all test groups to provide an overview of the real differences between groups and variabilities in each group. In the PCA scores plot (Figure 2A,C), a rough separation was visible between control and Zn-exposed groups, indicating altered metabolic profiles in *E. crypticus* under different treatments. Clear separation was observed between acute (2d) and chronic (7d) exposure groups along the first principle axis. This highlighted the importance of exposure time for metabolic reprogramming. It has been reported that the baseline metabolite changes spanning the normal growth stages of *Daphnia similis* exhibited a rapid and dynamic pattern.<sup>23</sup> Hence, in our study, the changes in metabolic profiles due to ZnO-NPs and ZnCl<sub>2</sub> treatments were compared with their matched controls at the same exposure duration.

Supervised PLS-DA was further employed on all test groups to maximize the separation between groups and to find the responsible metabolites leading to this separation. In the PLS-DA scores plot (Figure 2B,D), the low-dose ZnO-NPs groups (ZnO\_10\_2d and ZnO\_10\_7d) were gathered together with their corresponding control groups (Control\_2d and Control\_7d), whereas high-dose ZnO-NPs groups and all ZnCl<sub>2</sub>-exposed groups were well separated from their corresponding control groups. This suggested a dose-dependent and metal form-dependent manner of metabolic responses. For all test

groups, a total of 107 and 57 significantly changed metabolites (SCMs; VIP > 1 and  $p < 0.05$ ) under positive and negative mode, respectively, were determined. To globally characterize metabolic perturbations of *E. crypticus*, the normalized mass spectral signal intensities of the SCMs in all exposure groups were subjected to hierarchical clustering (Figure 3). Upon increasing exposure levels and exposure time, the differences in expression patterns of metabolites between control and Zn-exposed groups became more apparent, whereas the differences between ZnO-NPs and ZnCl<sub>2</sub> groups became smaller.

To further focus on the key differences between Zn forms while removing the time influence, we compared the metabolic responses of ZnO-NPs versus ZnCl<sub>2</sub> at an equivalent concentration of Zn and at a single time point (Figure 4). Generally, there was an apparent separation between ZnO-NPs- and ZnCl<sub>2</sub>-exposed groups for all four comparisons. Low dose of ZnO-NPs (10 mg/L) did not induce significant metabolic changes as compared to the control at day 2, but the distinct metabolic responses were observed at day 7. At the same exposure level of Zn, the metabolic response of *E. crypticus* to ZnO-NPs was less pronounced than that to ZnCl<sub>2</sub> (Figures 3 and 4), despite the (slightly) higher body concentration in ZnO-NPs treatments. This echoed the findings that ZnO-NPs generally had less impact than ZnCl<sub>2</sub> on life history traits and immune activity of the earthworm, *Eisenia veneta* under an equivalent Zn exposure.<sup>41</sup> Given the fact that body Zn concentrations were slightly higher for ZnO-NPs treatments, certain aspects of NP structure or behavior may play a role in alleviating their toxicity even when accumulated in the organism. For instance, ZnO-NPs could remain as particles and not dissolve in the animal tissues to release Zn ions. These findings also suggests that the released Zn<sup>2+</sup> may be the primary contributors to the toxicity of ZnO-NPs.

**Metabolites Altered in Different Exposure Groups and Their Biological Functions.** In order to elucidate the molecular toxicity and detoxification mechanisms of metal ions and nanoparticles and to determine how time may affect the nature of difference in metabolic profiles between the different Zn forms, we conducted PLS-DA for control versus ZnO-

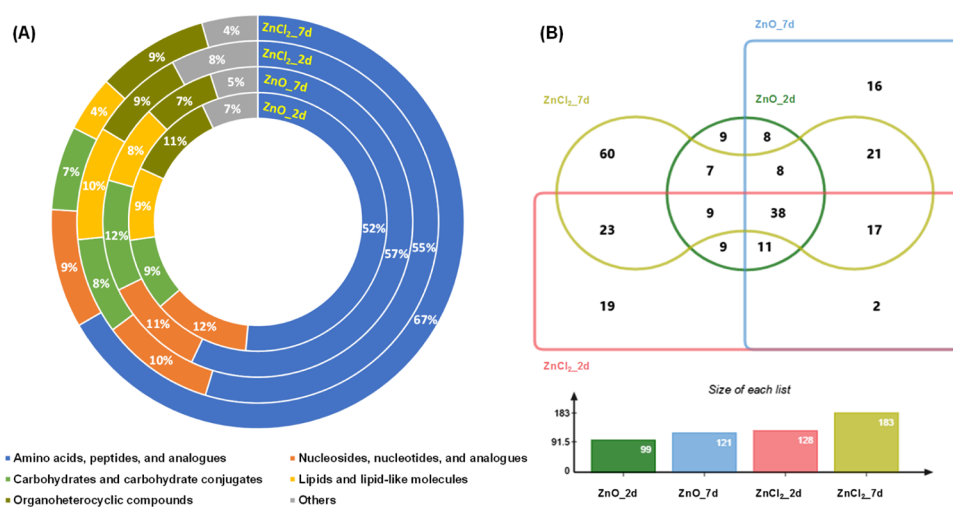


**Figure 5.** Proportion of SCMs in different categories after 2 and 7 days of exposure to ZnO-NPs and ZnCl<sub>2</sub> (A) and the Edwards–Venn diagram of the total number of SCMs (B). The total numbers of SCMs in ZnO\_2d, ZnO\_7d, ZnCl<sub>2</sub>\_2d, and ZnCl<sub>2</sub>\_7d groups were 99, 121, 128, and 183, respectively. The SCMs were obtained by conducting PLS-DA analyses for each Zn-exposed group vs the matched control group (VIP > 1 and  $p < 0.05$ ). Note: the metabolites identified from the positive ion mode and negative ion mode were merged together.

exposed samples and control versus ZnCl<sub>2</sub>-exposed samples at each time point separately (Figures S2–S5). The metabolites identified from the positive ion mode and negative ion mode were merged together. This step allowed determining 99, 128, 121, and 183 SCMs (VIP > 1 and  $p < 0.05$ ) in *E. crypticus* exposed to ZnO-NPs for 2 d, ZnCl<sub>2</sub> for 2 d, ZnO-NPs for 7 d, and ZnCl<sub>2</sub> for 7 d, respectively (Tables S4–S7). Generally, these SCMs could be classified into the following categories: (I) amino acids, peptides, and analogues, (II) nucleosides, nucleotides, and analogues, (III) carbohydrates and carbohydrate conjugates, (IV) lipids and lipid-like molecules, (V) organoheterocyclic compounds, and (VI) others. The proportion of the SCMs in different categories is depicted in Figure 5A. In all exposure groups, more than half (52–67%) of the SCMs belonged to category I (mainly dipeptides), whereas the proportions of the SCMs in each of the other four categories were between 4 and 12%. In accordance with the number and fold changes of differential metabolites (Tables S4–S7), ZnCl<sub>2</sub>\_7d had the greatest impact on the magnitude and spectrum of metabolic reprogramming, followed by ZnCl<sub>2</sub>\_2d, ZnO\_7d, and ZnO\_2d. An Edwards–Venn diagram was constructed to show the overlapping and specific SCMs after exposure to ZnO-NPs and ZnCl<sub>2</sub> (Figure 5B). A total of 38 SCMs were shared by all four exposure groups. There were 67 and 84 overlapping SCMs between ZnO-NPs and ZnCl<sub>2</sub> groups at day 2 and day 7, respectively. Approximately 30% of SCMs in ZnO\_2d (32 out of 99) and ZnO\_7d (37 out of 121) groups were nanospecific. Our results thus suggested that both nanoparticles and released ions contributed to the toxicity of ZnO-NPs at the metabolic level. The SCMs in different exposure groups were further interpreted according to their biological functions.

**Oxidative Stress and Antioxidant Defense.** Alterations in glutathione disulfide (GSSG), L-pyroglutamic acid, and 5-L-glutamyl-L-alanine were observed in all exposure groups (Tables S4–S7). These metabolites are known to participate in glutathione metabolism. GSH and GSSG are biologically important intracellular thiols, and alterations in the ratio between GSH and GSSG (oxidative stress index) are often used to assess exposure of cells to oxidative stress.<sup>42</sup> A strong

downregulation (up to 2.9-fold) of L-carnosine was observed in all exposure groups except ZnO\_2d (Tables S4–S7). L-carnosine (beta-alanyl-L-histidine) is a dipeptide with antioxidant activity and found exclusively in animal tissues.<sup>43,44</sup> Xu et al.<sup>45</sup> reported that L-carnosine levels increased in the tea tree oil-treated *Botrytis cinerea* as a protective response against H<sub>2</sub>O<sub>2</sub>-induced oxidative stress. In the present study, the antioxidant enzyme activities (SOD, POD, and CAT) and the contents of GSH and MDA in the worms were further determined (Figure 1C,G). Changes in the activity of SOD, POD, and CAT showed inconsistent patterns; however, a larger increase or decrease was generally observed in high-dose and long-term exposures. The depletion of GSH was observed upon exposure. GSH can scavenge excess ROS and be oxidized to GSSG.<sup>42</sup> The levels of MDA were increased in the Zn exposed samples. MDA is generated during lipid peroxidation, serving as a marker of oxidative stress.<sup>46</sup> In a previous study, the activity of SOD in fresh water mussels (*Unio tumidus*) was significantly elevated after exposure to Zn<sup>2+</sup> and ZnO-NPs.<sup>47</sup> At the genomic level, the upregulation of oxidative stress-related genes in *Arabidopsis thaliana* was observed upon exposure to Cu<sup>2+</sup> and CuO-NPs.<sup>48</sup> The present study, together with previous toxicological studies performed at different levels of biological organization, points to the activation of cellular antioxidant processes for protecting organisms against nanotoxicity.

**Membrane Disturbance.** Exposure to ZnO-NPs and ZnCl<sub>2</sub> generally induced a decrease in phosphatidylcholine, glycerophosphocholine, and phosphorylcholine and an increase in glycerol 3-phosphate and sn-glycerol 3-phosphoethanolamine. All of these metabolic shifts are indicative of Zn-induced disruption of glycerophospholipid metabolism, which is closely correlated to the membrane state.<sup>26</sup> Phosphatidylcholines are key components of the lipid bilayer of cells.<sup>49</sup> Phosphatidylcholines can be reversely converted to glycerophosphocholine.<sup>50</sup> Phosphorylcholine is the only phospholipid of the membrane that is not built with a glycerol backbone. Glycerol 3-phosphate and sn-glycerol 3-phosphoethanolamine are the downstream products of glycerophospholipid metabolism. Increased levels of phosphorylcholine-containing lipids in the

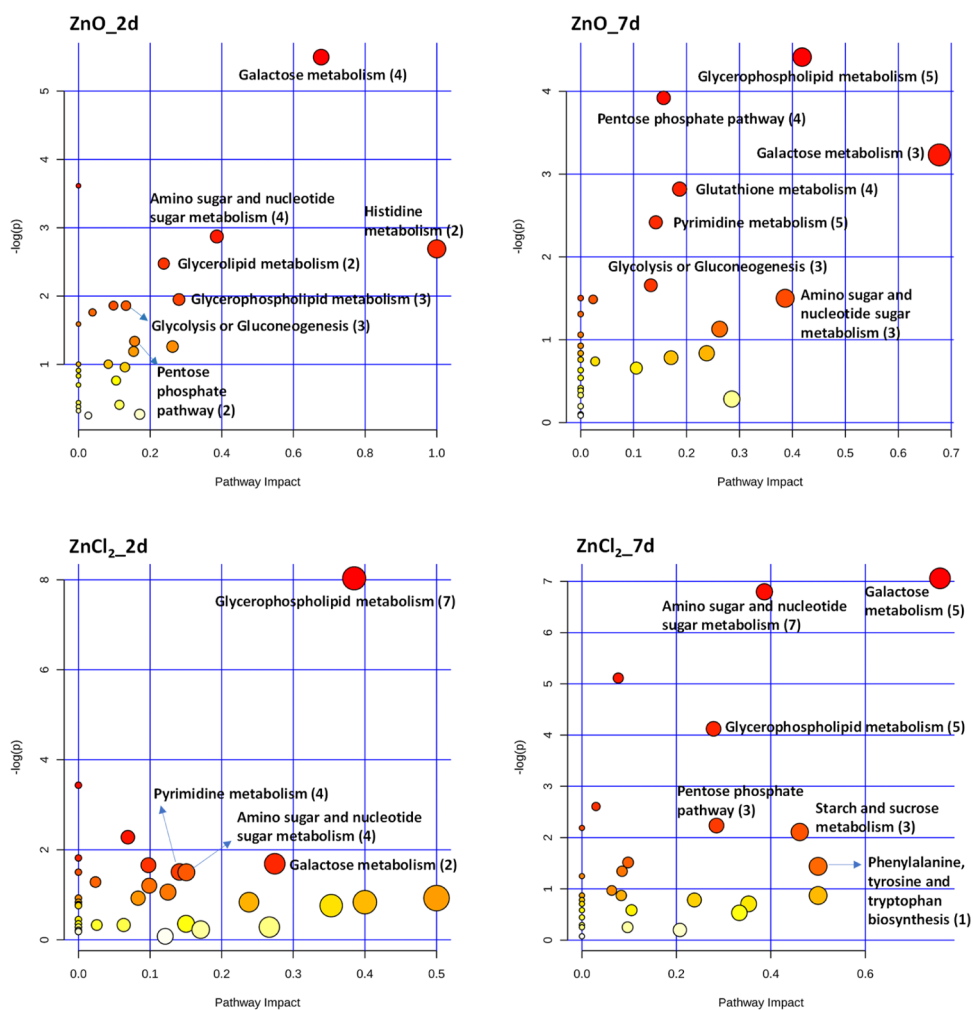


**Figure 6.** Pathway analysis of *E. crypticus* exposed to ZnO-NPs and ZnCl<sub>2</sub> for 2 and 7 days, respectively. The number of involved metabolites in each pathway are indicated in brackets. The pathways with  $p$  value < 0.05 (enrichment analysis) and impact value > 0.1 (pathway topology analysis) were considered as potentially affected. See Tables S8 and S9 for details.

lung tissues and decreased levels of glycerophosphocholine in the bronchoalveolar lavage fluid of rats were observed after ZnO-NPs exposure.<sup>50</sup> In our study, the unsaturated fatty acids alpha-linolenic acid, linoleic acid, and arachidonic acid were significantly downregulated in ZnO\_2d and ZnCl<sub>2</sub>\_2d groups, but not in the 7-day exposure groups (Tables S4–S7). Alpha-linolenic acid is an important structural component of the cell membrane. When incorporated into phospholipids, they affect cell membrane properties such as fluidity, flexibility, permeability, and the activity of membrane-bound enzymes.<sup>51</sup> The downregulation of linolenic and linoleic acids was also observed in cucumber (*Cucumis sativus*) after AgNPs and Ag<sup>+</sup> treatments.<sup>26</sup> A few other fatty acids, including azelaic acid, palmitic acid, valeric acid, mevalonic acid, *cis*-9-palmitoleic acid, oleic acid, capric acid, dodecanoic acid, and citraconic acid, were up- or downregulated depending on metal forms and exposure time (Tables S4–S7). One possible explanation for the differential expressions of fatty acids is lipid peroxidation leading to membrane damage. Another possibility is that animals adjust the membrane composition to maintain/rebuild the stability and integrity of the membrane. To prove the effects of Zn exposure on membrane permeability, we performed PI staining in the worms. PI is highly fluorescent when bound to nucleic acids. It is membrane-impermeable and

therefore cannot stain normal cells. The fluorescence images and the relative fluorescence intensity of the exposed worms are shown in Figures S6 and 1L. The degree of membrane damage, as reflected from the fluorescence intensity, was exacerbated with increasing exposure concentration and time. The fluorescence intensity was higher in ZnCl<sub>2</sub> than in ZnO-NPs treatments upon acute exposure, whereas the fluorescence intensity was identical in the worms exposed to different Zn forms at equivalent Zn concentration upon chronic exposure. The membrane damage by nanoparticles has also been proven before. For instance, polystyrene latex nanoparticles induced severe damage and holes on the cell membrane as revealed by hopping probe ion conductance microscopy.<sup>52</sup> These findings imply that nanoparticles can change the membrane state either directly or indirectly by interfering with membrane lipid biosynthesis and fatty acid composition.

**Energy Expenditure.** The response of organisms to metals may be also reflected by the alteration of energy reserves because additional energy is required for stress resistance, such as the maintenance of basal metabolism for survival and reproduction and metal detoxification.<sup>53,54</sup> In the present study, the energy-related metabolites, such as adenine, glycerol 3-phosphate, and glucose 1-phosphate, were significantly affected by ZnO-NPs and ZnCl<sub>2</sub> exposures (Tables S4–S7).

Adenine forms adenosine, a nucleoside, which further forms adenosine triphosphate (ATP) when three phosphate groups are added to adenosine. Glycerol 3-phosphate is a chemical substance which can be utilized for production of energy in the organism. Glucose 1-phosphate could be interconverted by the enzyme phosphoglucomutase to become glucose 6-phosphate. Free glucose 1-phosphate can also react with uridine triphosphate (UTP) to form the active nucleotide, uridine diphosphate glucose (UDP-glucose) (glucose-1-phosphate + UTP  $\rightleftharpoons$  UDP-glucose + pyrophosphate). An obvious decrease of uridine diphosphategalactose (UDPgal) was found in both ZnO-NP and ZnCl<sub>2</sub> treatments, with approximately 2-fold changes. UDPgal is a nucleoside diphosphate sugar, which joins in the galactose metabolism and amino sugar and nucleotide sugar metabolism. Furthermore, the impacts of different Zn forms on the energy budget of *E. crypticus* were assessed using the total content of glycogen, lipids (NEFA), and proteins and the activity of ATPase as indicators (Figure 1H,J). The Zn exposures induced an obvious reduction of NEFA and protein reserves and an inhibition of ATPase, whereas the content of glycogen was not affected. When looking at the NEFA contents, a greater reduction in NEFA was observed in ZnCl<sub>2</sub> treatments than in ZnO-NPs treatments at day 2 and this difference became smaller at day 7. Adam et al.<sup>55</sup> also reported the reduced energy reserves (lipids and proteins) of *Daphnia magna* exposed to CuO-NPs. Upon exposure to Cd and Zn, the lipid contents in *E. albidus* decreased with increasing exposure concentration and time, but the reduction of carbohydrate content was only found after 4–8 days of exposure. These nontargeted and targeted analyses clearly demonstrated that the energy metabolism of *E. crypticus* was disturbed by the Zn exposures and these effects were time-dependent.

**Metabolite Changes Specific to ZnO-NPs.** There were eight metabolites that were significantly regulated by both ZnO\_2d and ZnO\_7d, but not ZnCl<sub>2</sub> treatments (Figure 5B). Using a more rigorous cutoff of VIP > 1.5, two interesting metabolites (ergothioneine and riboflavin) were screened out and can potentially be used as early warning signs of ZnO-NPs toxicity. Ergothioneine is an important active material in the body with many physiological functions, such as scavenging free radicals, detoxification, maintaining DNA biosynthesis, normal growth of cells, and cellular immunity.<sup>47,56</sup> Moreover, ergothioneine could protect DNA mitochondrial components from the damage from electron-transferred ROS, helping to maintain the structure and function of mitochondria. As mitochondria are important sites for ATP synthesis, ergothioneine is directly related to the energy supply of various life activities in cells.<sup>57</sup> In our study, compared to the control, a notable decrease (1.5 to 2-fold changes) in the abundance of ergothioneine was observed after ZnO-NP exposures, implying a nonspecific effect on antioxidant activity and energy supply of *E. crypticus*. Riboflavin is one of the nutrients that could act as an antioxidant against oxidative stress of organisms, especially lipid peroxidation. Some animal studies have indicated that riboflavin status can affect the activity of antioxidant enzymes including GSH-Px, SOD, and CAT.<sup>58,59</sup> In addition, riboflavin has been shown to be a constituent of two coenzymes, flavin mononucleotide and flavin adenine dinucleotide, which are involved in the energy metabolism of organisms. It is thus speculated that the downregulation of riboflavin in the present study played an important role in ZnO-NP-introduced toxicity.

**Perturbed Metabolic Pathways in *E. crypticus* Exposed to ZnO-NPs and ZnCl<sub>2</sub>.** It is generally acknowledged that metabolite changes occurring at important positions of biological networks cause more severe impact on the pathways than the changes which occur in relatively isolated positions.<sup>53</sup> Here, metabolic pathway analysis revealed significant perturbations of a total of 11 biological pathways for different exposure groups (i.e., ZnO\_2d, ZnO\_7d, ZnCl<sub>2</sub>\_2d, and ZnCl<sub>2</sub>\_7d) (Figure 6, Tables S8 and S9). All four groups induced perturbation of three pathways, including galactose metabolism, amino sugar and nucleotide sugar metabolism, and glycerophospholipid metabolism. Both ZnO\_2d and ZnO\_7d groups perturbed seven biological pathways, of which five overlapped (galactose metabolism, amino sugar and nucleotide sugar metabolism, glycerophospholipid metabolism, glycolysis or gluconeogenesis, and pentose phosphate pathway), two were specific to ZnO\_2d (histidine metabolism and glycerolipid metabolism), and two were specific to ZnO\_7d (glutathione metabolism and pyrimidine metabolism). The ZnCl<sub>2</sub>\_2d and ZnCl<sub>2</sub>\_7d groups induced perturbation of four and six pathways, respectively. Glycerophospholipid metabolism, galactose metabolism, and amino sugar and nucleotide sugar metabolism disturbances were observed in both 2 and 7 d exposure groups. In addition, pyrimidine metabolism was perturbed in ZnCl<sub>2</sub>\_2d-exposed groups, whereas the pentose phosphate pathway, starch and sucrose metabolism, and phenylalanine, tyrosine, and tryptophan biosynthesis were affected in the ZnCl<sub>2</sub>\_7d-exposed groups. These findings indicate that responses to ZnO-NPs and ZnCl<sub>2</sub> at different exposure durations involve both common and specific pathways, but, in general, the toxicity of metal-based NPs may result from a synergistic action of the metal ions and nanoparticles.<sup>19</sup> Based on the involvement frequency in metabolism pathways (Tables S8 and S9) and biological function importance of metabolites, glucose-1-phosphate, glycerol 3-phosphate, and phosphorylcholine could serve as the potential biomarkers of different forms of Zn exposure in *E. crypticus*.

**Implications.** The present study investigated the molecular-level toxicodynamic processes of ZnO-NPs and ZnCl<sub>2</sub> in a soil sentinel species, *E. crypticus* using a high throughput metabolomics approach. The results showed that exposure to NPs under environmentally relevant concentrations caused substantial metabolic toxicity, although visible symptoms were not observed at these doses. The metabolic shifts of *E. crypticus* in response to ZnCl<sub>2</sub> were more pronounced than the responses to ZnO-NPs at equivalent Zn exposures. More evident metabolic reprogramming was observed with prolonged exposure time, especially for low-dose treatments. This suggests that dose-response and time-series measurements are essential for discovering modes of action of metal and metal-based NPs. The nontargeted metabolomics, complemented by the targeted analysis, revealed that Zn, both in nanoparticulate and ionic form affected the antioxidant system, the membrane protection, and the energy metabolism of *E. crypticus*. Metabolites (30% of total SCMs) responding solely to ZnO-NPs were identified, proving the existence of nanospecific toxicity. Putative perturbed biological pathways were determined by impact analysis, providing insights into the underlying mechanisms of toxicity of different Zn forms. Further investigations into the activities of crucial enzymes regulating the specific pathways or into the use of multi-omics tools may help to confirm the results of the metabolic analysis.

Nevertheless, metabolomics provides a direct and functional measure of the organism's response at the molecular level, therefore accelerating the construction of AOPs of NPs. A more practical insight that arises from omics-based studies is related to the possibilities to develop new strategies and predictive tools for assessing exposure and effects of NPs in soil animals.

## ■ ASSOCIATED CONTENT

### SI Supporting Information

The Supporting Information is available free of charge at <https://pubs.acs.org/doi/10.1021/acs.est.0c00663>.

Total ion chromatograms of the QC samples, PCA and PLS-DA analysis of selected test groups and results of fluorescence imaging of worms, hydrodynamic diameters of ZnO-NPs, the dissolution dynamics of ZnO-NPs, the estimated uptake, and depuration rate constants of ZnO-NPs and ZnCl<sub>2</sub>, SCMs in different exposure groups, and the outputs of pathway analysis (PDF)

## ■ AUTHOR INFORMATION

### Corresponding Author

**Hao Qiu** – School of Environmental Science and Engineering, Shanghai Jiao Tong University, Shanghai 200240, China; Guangdong Provincial Key Laboratory of Environmental Pollution Control and Remediation Technology, Sun Yat-sen University, Guangzhou 510275, China; [orcid.org/0000-0002-4743-9702](https://orcid.org/0000-0002-4743-9702); Email: [haoqiu@sjtu.edu.cn](mailto:haoqiu@sjtu.edu.cn)

### Authors

**Erkai He** – School of Environmental Science and Engineering, Shanghai Jiao Tong University, Shanghai 200240, China; School of Environmental Science and Engineering, Sun Yat-sen University, Guangzhou 510275, China; [orcid.org/0000-0002-4866-3001](https://orcid.org/0000-0002-4866-3001)

**Rongliang Qiu** – School of Environmental Science and Engineering, Sun Yat-sen University, Guangzhou 510275, China

**Xinde Cao** – School of Environmental Science and Engineering, Shanghai Jiao Tong University, Shanghai 200240, China; [orcid.org/0000-0002-2315-4219](https://orcid.org/0000-0002-2315-4219)

**Lan Song** – School of Environmental Science and Engineering, Southern University of Science and Technology, Shenzhen 518055, China

**Willie J.G.M. Peijnenburg** – National Institute of Public Health and the Environment, Center for the Safety of Substances and Products, Bilthoven 3720 BA, The Netherlands

Complete contact information is available at: <https://pubs.acs.org/10.1021/acs.est.0c00663>

### Notes

The authors declare no competing financial interest.

## ■ ACKNOWLEDGMENTS

This work was funded by the National Natural Science Foundation of China (no. 41877500, no. 41701573, no. 41701571, and no. 41977115), the Key Laboratory of Original Agro-Environmental Pollution Prevention and Control, Ministry of Agriculture/Tianjin Key Laboratory of Agro-environment and Safe-product (no. 17Z1170010019), and the Research Fund Program of Guangdong Provincial Key

Laboratory of Environmental Pollution Control and Remediation Technology (no. 2018K01).

## ■ REFERENCES

- (1) Dimkpa, C. O.; Latta, D. E.; McLean, J. E.; Britt, D. W.; Boyanov, M. I.; Anderson, A. J. Fate of CuO and ZnO Nano- and Microparticles in the Plant Environment. *Environ. Sci. Technol.* **2013**, *47*, 4734–4742.
- (2) Ma, H.; Williams, P. L.; Diamond, S. A. Ecotoxicity of manufactured ZnO nanoparticles—A review. *Environ. Pollut.* **2013**, *172*, 76–85.
- (3) Rajput, V.; Minkina, T.; Sushkova, S.; Behal, A.; Maksimov, A.; Blicharska, E.; Ghazaryan, K.; Movsesyan, H.; Barsova, N. ZnO and CuO nanoparticles: a threat to soil organisms, plants, and human health. *Environ. Geochem. Health* **2020**, *42*, 147–158.
- (4) Cornelis, G.; Hund-Rinke, K.; Kuhlbusch, T.; Van den Brink, N.; Nickel, C. Fate and bioavailability of engineered nanoparticles in soils: a review. *Crit. Rev. Environ. Sci. Technol.* **2014**, *44*, 2720–2764.
- (5) Gottschalk, F.; Sun, T.; Nowack, B. Environmental concentrations of engineered nanomaterials: Review of modeling and analytical studies. *Environ. Pollut.* **2013**, *181*, 287–300.
- (6) Vale, G.; Mehennaoui, K.; Cambier, S.; Libralato, G.; Jomini, S.; Domingos, R. F. Manufactured nanoparticles in the aquatic environment-biochemical responses on freshwater organisms: A critical overview. *Aquat. Toxicol.* **2016**, *170*, 162–174.
- (7) He, E.; Qiu, H.; Huang, X.; Van Gestel, C. A. M.; Qiu, R. Different dynamic accumulation and toxicity of ZnO nanoparticles and ionic Zn in the soil sentinel organism *Enchytraeus crypticus*. *Environ. Pollut.* **2019**, *245*, 510–518.
- (8) Lopes, S.; Ribeiro, F.; Wojnarowicz, J.; Łojkowski, W.; Jurkschat, K.; Crossley, A.; Soares, A. M. V. M.; Loureiro, S. Zinc oxide nanoparticles toxicity to *Daphnia magna*: size-dependent effects and dissolution. *Environ. Toxicol. Chem.* **2014**, *33*, 190–198.
- (9) Franklin, N. M.; Rogers, N. J.; Apte, S. C.; Batley, G. E.; Gadd, G. E.; Casey, P. S. Comparative toxicity of nanoparticulate ZnO, bulk ZnO, and ZnCl<sub>2</sub> to a freshwater microalga (*Pseudokirchneriella subcapitata*): the importance of particle solubility. *Environ. Sci. Technol.* **2007**, *41*, 8484–8490.
- (10) Xiao, Y.; Vijver, M. G.; Chen, G.; Peijnenburg, W. J. G. M. Toxicity and accumulation of Cu and ZnO nanoparticles in *Daphnia magna*. *Environ. Sci. Technol.* **2015**, *49*, 4657–4664.
- (11) Bhuvaneshwari, M.; Iswarya, V.; Nagarajan, R.; Chandrasekaran, N.; Mukherjee, A. Acute toxicity and accumulation of ZnO NPs in *Ceriodaphnia dubia*: Relative contributions of dissolved ions and particles. *Aquat. Toxicol.* **2016**, *177*, 494–502.
- (12) Lin, L.; Xu, M.; Mu, H.; Wang, W.; Sun, J.; He, J.; Qiu, J.-W.; Luan, T. Quantitative proteomic analysis to understand the mechanisms of zinc oxide nanoparticle toxicity to *Daphnia pulex* (Crustacea: Daphniidae): comparing with bulk zinc oxide and zinc salt. *Environ. Sci. Technol.* **2019**, *53*, 5436–5444.
- (13) Świątek, Z. M.; van Gestel, C. A. M.; Bednarska, A. J. Toxicokinetics of zinc-oxide nanoparticles and zinc ions in the earthworm *Eisenia andrei*. *Ecotoxicol. Environ. Saf.* **2017**, *143*, 151–158.
- (14) Topuz, E.; van Gestel, C. A. M. Toxicokinetics and toxicodynamics of differently coated silver nanoparticles and silver nitrate in *Enchytraeus crypticus* upon aqueous exposure in an inert sand medium. *Environ. Toxicol. Chem.* **2015**, *34*, 2816–2823.
- (15) Waalewijn-Kool, P. L.; Rupp, S.; Lofts, S.; Svendsen, C.; van Gestel, C. A. M. Effect of soil organic matter content and pH on the toxicity of ZnO nanoparticles to *Folsomia candida*. *Ecotoxicol. Environ. Saf.* **2014**, *108*, 9–15.
- (16) Groh, K. J.; Carvalho, R. N.; Chipman, J. K.; Denslow, N. D.; Halder, M.; Murphy, C. A.; Roelofs, D.; Rolaki, A.; Schirmer, K.; Watanabe, K. H. Development and application of the adverse outcome pathway framework for understanding and predicting chronic toxicity: I. Challenges and research needs in ecotoxicology. *Chemosphere* **2015**, *120*, 764–777.

- (17) Du, C.; Zhang, B.; He, Y.; Hu, C.; Ng, Q. X.; Zhang, H.; Ong, C. N.; ZhifenLin. Biological effect of aqueous C60 aggregates on *Scenedesmus obliquus* revealed by transcriptomics and non-targeted metabolomics. *J. Hazard. Mater.* **2017**, *324*, 221–229.
- (18) Zhang, X.; Xia, P.; Wang, P.; Yang, J.; Baird, D. J. Omics advances in ecotoxicology. *Environ. Sci. Technol.* **2018**, *52*, 3842–3851.
- (19) Ruotolo, R.; Maestri, E.; Pagano, L.; Marmiroli, M.; White, J. C.; Marmiroli, N. Plant response to metal-containing engineered nanomaterials: an omics-based perspective. *Environ. Sci. Technol.* **2018**, *52*, 2451–2467.
- (20) Landa, P.; Prerostova, S.; Petrova, S.; Knirsch, V.; Vankova, R.; Vanek, T. The transcriptomic response of *Arabidopsis thaliana* to zinc oxide: a comparison of the impact of nanoparticle, bulk, and ionic zinc. *Environ. Sci. Technol.* **2015**, *49*, 14537–14545.
- (21) Lankadurai, B. P.; Nagato, E. G.; Simpson, M. J. Environmental metabolomics: an emerging approach to study organism responses to environmental stressors. *Environ. Rev.* **2013**, *21*, 180–205.
- (22) Ryan, D.; Robards, K. Metabolomics: The greatest omics of them all? *Anal. Chem.* **2006**, *78*, 7954–7958.
- (23) Zhang, B.; Zhang, H.; Du, C.; Ng, Q. X.; Hu, C.; He, Y.; Ong, C. N. Metabolic responses of the growing *Daphnia similis* to chronic AgNPs exposure as revealed by GC-Q-TOF/MS and LC-Q-TOF/MS. *Water Res.* **2017**, *114*, 135–143.
- (24) Zhang, J. L.; Zhou, Z. P.; Pei, Y.; Xiang, Q. Q.; Chang, X. X.; Ling, J.; Shea, D.; Chen, L. Q. Metabolic profiling of silver nanoparticle toxicity in *Microcystis aeruginosa*. *Environ. Sci.: Nano* **2018**, *5*, 2519–2530.
- (25) Zhang, H.; Lu, L.; Zhao, X.; Zhao, S.; Gu, X.; Du, W.; Wei, H.; Ji, R.; Zhao, L. Metabolomics reveals the “invisible” responses of spinach plants exposed to CeO<sub>2</sub> nanoparticles. *Environ. Sci. Technol.* **2019**, *53*, 6007–6017.
- (26) Lu, T.; Ke, M.; Peijnenburg, W. J. G. M.; Zhu, Y.; Zhang, M.; Sun, L.; Fu, Z.; Qian, H. Investigation of rhizospheric microbial communities in wheat, barley, and two rice varieties at the seedling stage. *J. Agric. Food Chem.* **2018**, *66*, 2645–2653.
- (27) Holden, P. A.; Klaessig, F.; Turco, R. F.; Priester, J. H.; Rico, C. M.; Avila-Arias, H.; Mortimer, M.; Pacpaco, K.; Gardea-Torresdey, J. L. Evaluation of exposure concentrations used in assessing manufactured nanomaterial environmental hazards: are they relevant? *Environ. Sci. Technol.* **2014**, *48*, 10541–10551.
- (28) Comfort, K. K.; Braydich-Stolle, L. K.; Maurer, E. I.; Hussain, S. M. Less is more: long-term in vitro exposure to low levels of silver nanoparticles provides new insights for nanomaterial evaluation. *ACS Nano* **2014**, *8*, 3260–3271.
- (29) Lankadurai, B. P.; Wolfe, D. M.; Simpson, A. J.; Simpson, M. J. <sup>1</sup>H NMR-based metabolomics of time-dependent responses of *Eisenia fetida* to sub-lethal phenanthrene exposure. *Environ. Pollut.* **2011**, *159*, 2845–2851.
- (30) Jager, T.; Albert, C.; Preuss, T. G.; Ashauer, R. General unified threshold model of survival - a toxicokinetic-toxicodynamic framework for ecotoxicology. *Environ. Sci. Technol.* **2011**, *45*, 2529–2540.
- (31) Castro-Ferreira, M. P.; Roelofs, D.; van Gestel, C. A. M.; Verweij, R. A.; Soares, A. M. V. M.; Amorim, M. J. B. *Enchytraeus crypticus* as model species in soil ecotoxicology. *Chemosphere* **2012**, *87*, 1222–1227.
- (32) Castro-Ferreira, M. P.; de Boer, T. E.; Vooijs, R.; van Gestel, C. A.; van Straalen, N. M.; Soares, A. M.; Amorim, M. J.; Roelofs, D.; Roelofs, D. Transcriptome assembly and microarray construction for *Enchytraeus crypticus*, a model oligochaete to assess stress response mechanisms derived from soil conditions. *BMC Genom.* **2014**, *15*, 302.
- (33) He, E.; van Gestel, C. A. M. Toxicokinetics and toxicodynamics of nickel in *Enchytraeus crypticus*. *Environ. Toxicol. Chem.* **2013**, *32*, 1835–1841.
- (34) Zhao, L.; Huang, Y.; Paglia, K.; Vaniya, A.; Wanciewicz, B.; Keller, A. A. Metabolomics reveals the molecular mechanisms of copper induced cucumber leaf (*Cucumis sativus*) senescence. *Environ. Sci. Technol.* **2018**, *52*, 7092–7100.
- (35) Xia, J.; Wishart, D. S. MSEA: a web-based tool to identify biologically meaningful patterns in quantitative metabolomic data. *Nucleic Acids Res.* **2010**, *38*, W71–W77.
- (36) Qiu, H.; Smolders, E. Nanospecific phytotoxicity of CuO nanoparticles in soils disappeared when bioavailability factors were considered. *Environ. Sci. Technol.* **2017**, *51*, 11976–11985.
- (37) Choi, M.-K.; Son, S.; Hong, M.; Choi, M. S.; Kwon, J. Y.; Lee, J. Maintenance of membrane integrity and permeability depends on a patched-related protein in *Caenorhabditis elegans*. *Genetics* **2016**, *202*, 1411–1420.
- (38) McCarty, L. S.; Mackay, D. Enhancing ecotoxicological modeling and assessment. body residues and modes of toxic action. *Environ. Sci. Technol.* **1993**, *27*, 1718–1728.
- (39) Bednarska, A. J.; Stachowicz, I. Costs of living in metal polluted areas: respiration rate of the ground beetle *Pterostichus oblongopunctatus* from two gradients of metal pollution. *Ecotoxicology* **2013**, *22*, 118–124.
- (40) Bicho, R. C.; Santos, F. C. F.; Scott-Fordsmand, J. J.; Amorim, M. J. B. Effects of copper oxide nanomaterials (CuONMs) are life stage dependent - full life cycle in *Enchytraeus crypticus*. *Environ. Pollut.* **2017**, *224*, 117–124.
- (41) Hooper, H. L.; Jurkschat, K.; Morgan, A. J.; Bailey, J.; Lawlor, A. J.; Spurgeon, D. J.; Svendsen, C. Comparative chronic toxicity of nanoparticulate and ionic zinc to the earthworm *Eisenia veneta* in a soil matrix. *Environ. Int.* **2011**, *37*, 1111–1117.
- (42) Olsvik, P. A.; Kristensen, T.; Waagbø, R.; Rosseland, B. O.; Tollefsen, K.-E.; Baeverfjord, G.; Berntssen, M. H. G. mRNA expression of antioxidant enzymes (SOD, CAT and GSH-Px) and lipid peroxidative stress in liver of Atlantic salmon (*Salmo salar*) exposed to hyperoxic water during smoltification. *Comp. Biochem. Physiol., Part C: Toxicol. Pharmacol.* **2005**, *141*, 314–323.
- (43) Hipkiss, A. R. Carnosine and Its Possible Roles in Nutrition and Health. *Advances in Food and Nutrition Research*; Academic Press, 2009; Chapter 3, Vol. 57, pp 87–154.
- (44) Boldyrev, A. A.; Aldini, G.; Derave, W. Physiology and pathophysiology of carnosine. *Physiol. Rev.* **2013**, *93*, 1803–1845.
- (45) Xu, J.; Shao, X.; Li, Y.; Wei, Y.; Xu, F.; Wang, H. Metabolomic analysis and mode of action of metabolites of tea tree oil involved in the suppression of *Botrytis cinerea*. *Front. Microbiol.* **2017**, *8*, 1017.
- (46) Zhang, H.; Du, W.; Peralta-Videa, J. R.; Gardea-Torresdey, J. L.; White, J. C.; Keller, A.; Guo, H.; Ji, R.; Zhao, L. Metabolomics reveals how cucumber (*Cucumis sativus*) reprograms metabolites to cope with silver ions and silver nanoparticle-induced oxidative stress. *Environ. Sci. Technol.* **2018**, *52*, 8016–8026.
- (47) Gründemann, D. The ergothioneine transporter controls and indicates ergothioneine activity—A review. *Prev. Med.* **2012**, *54*, S71–S74.
- (48) Landa, P.; Dytrych, P.; Prerostova, S.; Petrova, S.; Vankova, R.; Vanek, T. Transcriptomic response of *Arabidopsis thaliana* exposed to CuO nanoparticles, bulk material, and ionic copper. *Environ. Sci. Technol.* **2017**, *51*, 10814–10824.
- (49) Guschina, I. A.; Harwood, J. L. Lipid metabolism in the moss *Rhytidiadelphus squarrosus* (Hedw.) Warnst. from lead-contaminated and non-contaminated populations. *J. Exp. Bot.* **2002**, *53*, 455–463.
- (50) Lee, S.-H.; Wang, T.-Y.; Hong, J.-H.; Cheng, T.-J.; Lin, C.-Y. NMR-based metabolomics to determine acute inhalation effects of nano- and fine-sized ZnO particles in the rat lung. *Nanotoxicology* **2016**, *10*, 924–934.
- (51) Zhao, L.; Zhang, H.; Wang, J.; Tian, L.; Li, F.; Liu, S.; Peralta-Videa, J. R.; Gardea-Torresdey, J. L.; White, J. C.; Huang, Y.; Keller, A.; Ji, R. C60 fullerenes enhance copper toxicity and alter the leaf metabolite and protein profile in cucumber. *Environ. Sci. Technol.* **2019**, *53*, 2171–2180.
- (52) Ruenraroengsak, P.; Novak, P.; Berhanu, D.; Thorley, A. J.; Valsami-Jones, E.; Gorelik, J.; Korchev, Y. E.; Tetley, T. D. Respiratory epithelial cytotoxicity and membrane damage (holes) caused by amine-modified nanoparticles. *Nanotoxicology* **2012**, *6*, 94–108.

(53) Ratnasekhar, C.; Sonane, M.; Satish, A.; Mudiam, M. K. R. Metabolomics reveals the perturbations in the metabolome of *Caenorhabditis elegans* exposed to titanium dioxide nanoparticles. *Nanotoxicology* **2015**, *9*, 994–1004.

(54) Sancho, E.; Villarroel, M. J.; Andreu, E.; Ferrando, M. D. Disturbances in energy metabolism of *Daphnia magna* after exposure to tebuconazole. *Chemosphere* **2009**, *74*, 1171–1178.

(55) Adam, N.; Vergauwen, L.; Blust, R.; Knapen, D. Gene transcription patterns and energy reserves in *Daphnia magna* show no nanoparticle specific toxicity when exposed to ZnO and CuO nanoparticles. *Environ. Res.* **2015**, *138*, 82–92.

(56) Dubost, N. J.; Beelman, R. B.; Peterson, D.; Royse, D. J. Identification and quantification of ergothioneine in cultivated mushrooms by liquid chromatography-mass spectroscopy. *Int. J. Med. Mushrooms* **2006**, *8*, 215–222.

(57) Addabbo, F.; Montagnani, M.; Goligorsky, M. S. Mitochondria and reactive oxygen species. *Hypertension* **2009**, *53*, 885–892.

(58) Panas, T.; Rungsun, T.; Panata, M.; Praneet, P.; Wichit, R.; Niyomsri, V.; Anchalee, T.; Benjaluck, P.; Supaporn, N. Antioxidant enzyme levels in the erythrocytes of riboflavin-deficient and *Trichinella spiralis*-infected rats. *Southeast Asian J. Trop. Med. Publ. Health* **2003**, *34*, 480–485.

(59) Ashoori, M.; Saedisomeolia, A. Riboflavin (vitamin B2) and oxidative stress: a review. *Br. J. Nutr.* **2014**, *111*, 1985–1991.